

Search for seismic discontinuities in the lower mantle

Lev Vinnik,^{1,2} Mamoru Kato^{1,3} and Hitoshi Kawakatsu¹

¹Earthquake Research Institute, University of Tokyo, 1-1-1 Yayoi, Bunkyo-ku, Tokyo 113-0032, Japan. E-mail: hitosi@eri.u-tokyo.ac.jp

²Institute of Physics of the Earth, B. Gruzinskaya 10, 123810 Moscow, Russia

³School of Earth Sciences, Faculty of Integrated Human Studies, Kyoto University, Kyoto, Japan

Accepted 2001 May 8. Received 2001 May 8; in original form 2000 July 24

SUMMARY

Indications of lower mantle discontinuities have been debated for decades, but still little is known about their properties, and their origins are enigmatic. In our study broad-band recordings of deep events are examined for the presence of signals from the lower-mantle discontinuities with a novel technique. We deconvolve vertical component of the *P*-wave coda in the period range around 10 s by the *S* waveform and stack many deconvolved traces with moveout time corrections. In synthetic seismograms for an earth model without lower mantle discontinuities, the strongest signal thus detected in the time window of interest is often *s*'410'*P* phase (generated as *S* and reflected as *P* from the '410 km' discontinuity above the source). In actual seismograms there are other phases that can be interpreted as converted from *S* to *P* at discontinuities in the lower mantle beneath the seismic source. We summarize the results of processing the seismograms (1) of deep events in Sunda arc at seismograph stations in east Asia, (2) deep Kermadec–Fiji–Tonga events at the J-array and FREESIA networks in Japan and stations in east Asia, and (3) deep events in the northwest Pacific region (Mariana, Izu-Bonin and the Japan arc) recorded at stations in north America. In our data there are indications of discontinuities near 860–880, 1010–1120, 1170–1250 and 1670–1800 km depths. The clearest signals are obtained from the discontinuity at a depth of 1200 km. We argue that the '900', '1200' and '1700 km' discontinuities are global, but laterally variable in both depth and strength. Seismic stratification of the lower mantle may have bearings on the patterns of subduction, as revealed by tomographic models.

Key words: array analysis, lower mantle, seismic discontinuities, stacking.

INTRODUCTION

Standard Earth models like IASP91 (Kennett & Engdahl 1991) contain discontinuities in the upper mantle, where seismic wave velocities and density change abruptly with depth. In contrast to the upper mantle models, the velocities in the lower mantle rise with depth with almost constant gradients. The only exception is a zone near the core–mantle boundary. However, there are reports, some of them published long ago, on discontinuities in the lower mantle. For example, Geiger & Gutenberg (1912) found indications of discontinuities near 1200 and 1700 km depths from the amplitude variations of the first arrivals. Mohorovicic (1916) found discontinuities at depths of 1200 and 1700 km from the analysis of travel times. Repetti (1930) observed a strong change of apparent *P* velocity at a distance of 33°. He attributed this change to a discontinuity near 970 km depth. To reconcile his data with the presently available upper-mantle velocity models, this discontinuity should be placed between 800 and 900 km depths. Quite a number of similar results were published later.

The discontinuities are important for geodynamics, geochemistry and mineral physics. If the lower mantle consists of

assemblages of (Mg, Fe) SiO₃ silicate perovskite and (Mg, Fe)O magnesiowustite, there are only some hypothetical possibilities to explain the discontinuities (Bina 1998), and the seismic data can be indicative of the properties and processes that are either overlooked or not well understood yet. Then why are the lower mantle discontinuities ignored in the earth models that are based on seismic data? There are a few reasons for this. The discontinuities in the lower mantle are weak and many indications of them should be rated unreliable. The traveltimes and amplitude variations with distance can in principle be caused not only by the radial but also by lateral velocity variations (e.g., Tromp & Dziewonski 1998). Some data on the lower mantle discontinuities were obtained about 30 years ago by direct measurements of *P*-wave slowness at seismic receiver arrays (Johnson 1969; Chinnery 1969; Greenfield & Sheppard 1969; Corbishley 1970; Vinnik & Nikolayev 1970; Vinnik *et al.* 1972). The data at different arrays are often different, which gives reasons to suspect that the data indeed are contaminated by the effects of lateral heterogeneity.

Recent developments in digital recording opened new possibilities for structural studies, and indications of discontinuities in the lower mantle were found in reflected (Petersen *et al.* 1993;

le Stunff *et al.* 1995) and *SdP* phases (converted from *S* to *P* at a depth '*d*' in the source region, Fig. 1). Short-period (1–2 s) *SdP* phases from discontinuities in the upper mantle were identified on short-period array recordings of deep events by Barley *et al.* (1982). Bock & Ha (1984) tentatively identified with this technique the phase converted from a discontinuity near 970 km depth in the Tonga region. Kawakatsu & Niu (1994) suggested that a discontinuity beneath the Tonga, Japan and Indonesia subduction zones at a depth of 920 km. Wicks & Richards (1993) concluded that on seismograms of the WRA short-period array in Australia there is a sequence of converted phases related to discontinuities at depths of 860, 1025 and 1200 km in the Fiji–Tonga region. Niu & Kawakatsu (1997) reported observations of phase converted at a depth of 1080 km in Indonesia. They suggested a large depth variation of this 'mid-mantle' discontinuity and its relation to the high velocity anomaly above the discontinuity. Kaneshima & Helffrich (1998) reported observations of phase scattered from *S* to *P* at a depth of around 1600 km in a vicinity of Mariana islands, and attributed this signal to a subducted slab (Kaneshima & Helffrich 1999).

Our analysis of *SdP* phases differs from the standard approach by using longer periods (around 10 s). The longer-period data are important, because some of the discontinuities apparently are not sharp enough to generate short-period reflected and converted phases. Moreover, in the longer-period range the records are not so much contaminated by randomly scattered waves, and the mantle becomes more transparent. Some of the short period scatterers, like those discussed by Wicks & Weber (1996) and Castle & Creager (2000) are interesting geophysical objects, but we must sacrifice them in order to proceed with our study of the lower-mantle discontinuities. The ultimate aim of our study is to check if previously reported evidence of the discontinuities can be confirmed with independent data and techniques. We want to broaden the geographical framework of previous studies and to find out if the discontinuities can be found only in a specific environment and thus are local, or they are global and can be found in different regions. Finally we want to find out if there is any relationship between the discontinuities and volumetric heterogeneities in the mantle, as found by tomographic studies.

Our technique of record processing (Vinnik *et al.* 1998) differs from the standard velocity filtering by elements of the

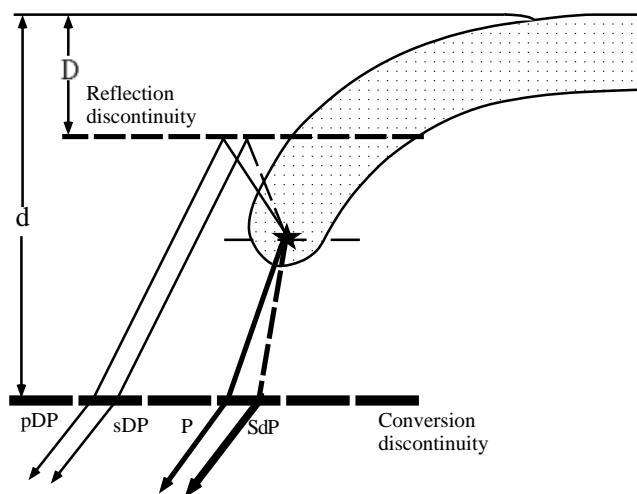


Figure 1. Ray paths of *SdP* and *sDP* phases.

receiver function approach. The conventional receiver function can be obtained by deconvolving the radial component of the *P*-wave record by the vertical component. To detect the *SdP* phases we deconvolve the vertical component of the *P*-wave coda by the *S* waveform and stack the resulting records of the same event at many stations with moveout corrections. The data obtained with this approach for deep events in the Sunda arc region were described earlier by Vinnik *et al.* (1998). Now these first results are complemented by the analysis of records of deep events in other regions. In the next Section we describe our technique; more details can be found in Vinnik *et al.* (1998). The technique is illustrated with the data for events in the Sunda arc region. Then we proceed to the data for the deep events in the Kermadec–Fiji–Tonga region and in the north-west Pacific region (Mariana, Izu-Bonin and the Japan arc). The map with epicentres and seismograph stations used is shown in Fig. 2, and the focal parameters of seismic events are listed in Table 1.

THE TECHNIQUE

SdP phases are polarized as *P* waves and recorded in the coda of the first arriving *P* wave. The delay of *SdP* phase relative to *P* phase is roughly proportional to the depth interval between the hypocentre and the converting interface; 1 s of delay is roughly equivalent to 10 km of depth (Fig. 3). There are two epicentral distance intervals where the mantle *SdP* phases of deep events can be observed without interference with stronger phases. One interval is between 30° and 50° . At smaller distances the *SdP* phases related to discontinuities deeper than about 1100 km do not exist. At distances around 50° the width of the time window for observing *SdP* phases is limited by the *PcP* arrivals. The other interval is at distances exceeding 67 – 68° . The window for observing *SdP* phases in this interval is bounded by the arrivals of *PcP* (at small times) and *pP* (at large times). In our study both distance interval are used, depending on the seismograph network available.

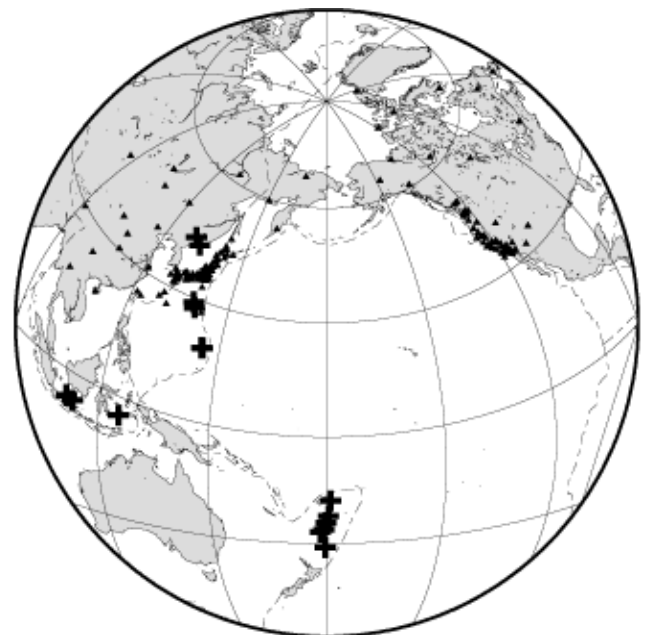


Figure 2. Epicentres (crosses) and seismograph stations (triangles).

Table 1. Parameters of the events.

Date	Time h:m:s	Lat deg	Lon deg	Depth km
Sunda arc				
1992 July 14	07:03:10.7	-4.71	125.43	477
1992 September 2	05:50:02.5	-6.04	112.14	636
1994 September 28	16:39:52.2	-5.77	110.33	643
1994 November 15	20:18:11.2	-5.61	110.20	559
Kermadec-Fiji-Tonga				
1993 August 7*	17:53:25.0	-23.76	179.96	526
1994 March 31*	22:40:54.2	-21.90	180.59	593
1994 October 27*	22:20:29.4	-25.71	179.46	523
1997 September 4*	04:23:36.1	-26.38	178.48	604
1997 March 21	12:07:17.6	-31.18	179.90	449
1998 March 29	19:48:16.2	-17.57	181.15	537
1998 May 16	02:22:03.2	-22.27	180.65	586
China-Russia border				
1994 July 21	18:36:31.7	42.30	133.04	473
1999 April 8	13:10:34.1	43.61	130.35	565
Mariana Islands				
1995 August 23	07:06:02.6	18.88	145.30	596
1995 August 24	01:55:39.3	18.93	145.19	589
Izu-Bonin Islands				
1996 March 16	22:04:06.2	29.12	139.12	477
1996 June 26	03:22:03.1	27.82	139.85	469

Events marked by * are relocated by Engdahl *et al.* (1998).

To detect the signal, the record of a deep event is decomposed into the vertical (Z), radial (R) and transverse (T or SH) components, low-pass filtered and deconvolved by the S waveform, taken preferably from the same record. Deconvolution is useful for two reasons. First, it enhances the phases, the waveform of which is similar to that of the S phase and suppresses the rest. Second, it eliminates differences between the source functions of different events and makes these records directly comparable. The corner period of the low-pass filter is usually taken near 10 s. Deconvolution is performed in time domain, with a proper

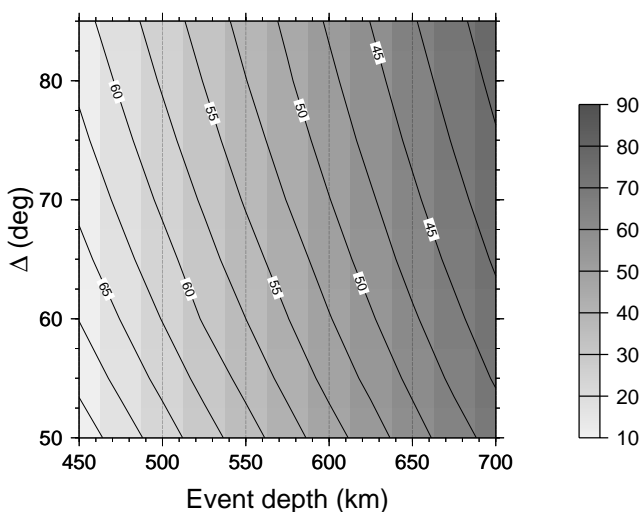


Figure 3. Dependence of arrival time relative to P phase on epicentral distance and depth of the event for $s^{410^\circ}P$ and $S^{1200^\circ}P$ phases. Time of $S^{1200^\circ}P$ is shown by isolines; numbers attached to isolines are times in seconds. Time of $s^{410^\circ}P$ is indicated by shading.

regularization. The S waveform is transformed by deconvolution into a ‘bump’. Origin of the time scale for the deconvolved trace is determined as $t_0 = (t_p - t_s) + t_d$, where t_p and t_s are the arrival times of the P and S waves, respectively, and t_d is the time of the top of the bump for the S wave; $(t_p - t_s)$ can be measured most accurately at short periods.

At distances exceeding 75° the S -wave group is composed of a few interfering phases (S , SKS , ScS). The records in this distance range are deconvolved by the S waveform observed at a smaller distance in the same azimuth from the epicentre. It is assumed that the observed SV waveform is similar to that which generates SdP phase, in spite of a 25° difference between their take-off angles and the effect of anelastic attenuation. A similarity of the waveforms of the recorded SV and of the parent SV for SdP is likely, if both are on the same side of the nodal line and far from it. Then the SdP waveform is transformed by deconvolution into a bump, as well. The time of the top of the bump is a delay of SdP relative to P . This bump can be enhanced by stacking the deconvolved traces at many stations with moveout time corrections.

Waveforms of SV and SH for the point dislocation source are similar except the sign and amplitude. If this similarity is present in actual events, the record can be deconvolved by either SV or SH waveform. The stronger component is preferable, because the other one can be distorted by coupling with the stronger component owing to shear-wave splitting in the upper mantle. The wave propagation theory (Aki & Richards 1980) predicts that at epicentral distances less than 50° the recorded SV wave is distorted by coupling with the inhomogeneous P wave which is formed at the Moho in a vicinity of the receiver, but in practice the distortion in the distance range between 30° and 50° is negligible. To suppress the strong P wave which is coupled with SV , the record of the S wave is projected on the axis which forms an angle of 40° with the vertical direction. This angle is found by trial and error.

The first-order moveout time corrections for stacking are calculated by multiplying the differential slowness by the differential distance. The differential slowness is determined relative to the first arriving P phase, and the differential distance is determined relative to the reference distance (average epicentral distance of the network). Our stack is linear, and we do not use any non-linear procedure. We avoid non-linear procedures for the following reasons. First, non-linear procedures are poorly studied theoretically and they can result in non-predictable effects. Second, non-linear procedures tend to suppress weak signals, whereas our interest is opposite. Finally, non-linear procedures distort waveforms, whereas we interpret the results of stacking with the aid of theoretical seismograms.

The deconvolved records are normalized to the amplitude of the parent SV for the SdP phases. We perform normalization by dividing the SdP amplitude by the amplitude of the S wave used for deconvolution and by correcting this ratio for the difference between the amplitudes of the S wave used for deconvolution and of the parent SV . The relationship between the amplitude of the parent SV and of the recorded S wave is determined from the focal mechanism of the earthquake. The amplitude normalized to the amplitude of the parent SV for SdP phases is termed ‘normalized amplitude’. The records are suitable for processing, if the corresponding theoretical amplitudes of the parent SV are not lower than 50 per cent of the maximum amplitude for the given focal mechanism. Otherwise the expected signal/noise ratio can be prohibitively low.

The bumps observed in the stack are regarded signals, if they are separated from the main *P*-wave group by a quiet interval, or if they differ from the main *P*-wave group by a dependence of the amplitude on differential slowness. The signal is detected reliably if its amplitude in the stack is comparable with the amplitudes of the individual traces. Then the signal detected in the stack should be seen in at least some of the individual traces. Sometimes an arrival in the stack is caused by arrivals at one or a few neighbouring stations, rather than by constructive interference of many records. Such arrivals can be recognized by a strong dependence of their time in the stack on differential slowness. By comparison, true signals are characterized by a nearly constant time in the slowness range corresponding to their largest amplitudes.

We compare the obtained stacks with the stacks of theoretical seismograms for IASP91 velocity model (Kennett & Engdahl 1991). Distribution of density is found from the standard scaling relationship and the medium is assumed to be without anelastic attenuation. The synthetics are calculated with a reflectivity technique (Fuchs & Mueller 1971) for the best double couple of the Harward CMT solution and for epicentral distances and azimuths of the real stations. The synthetics are processed like the real seismograms. Positive polarity of *SdP* phase means that at the discontinuity *S* velocity increases with depth.

As will be shown, the strongest signal in the theoretical stack for the standard earth model in the time window of interest is sometimes the *s*'410'*P* phase (Fig. 1), which is reflected as the *P* wave from the '410 km' discontinuity above the source. The phases converted beneath the source differ from those reflected above the source by slowness: the theoretical differential slowness of the *SdP* phases is negative, whereas that of the reflected phases is positive. The other criterion to distinguish between the phases reflected and converted in the source region is a different dependence of their times on focal depth. The delay of *SdP* phase relative to *P* is smaller for deeper events, whereas for the reflected phases the relation is opposite. In addition to reverberation in the source region, some arrivals can be caused by reverberation in the receiver region. The synthetics sometimes show distinct arrivals of *Pp*'410'*P* phase (*P* reflected from the Earth's surface and from a discontinuity at a depth of 410 km in the receiver region, Fig. 4). The delay of this phase relative to *P* is independent of event depth, and its differential slowness is positive.

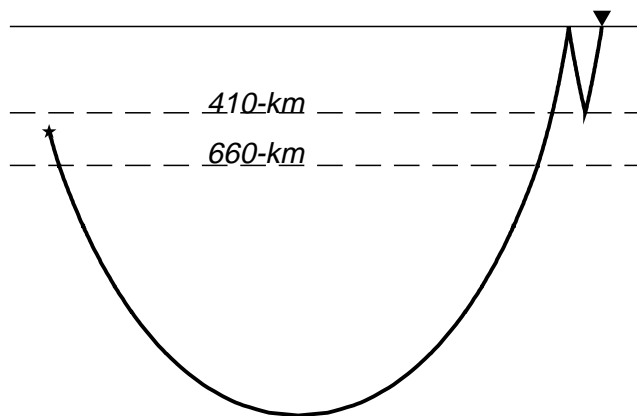


Figure 4. Raypath for *Pp*'410'*P* phase

EVENTS IN THE SUNDA ARC REGION

Signals interpreted as the *SdP* phases from lower-mantle discontinuities were identified with some confidence in the records of 4 events in the Sunda arc region (Vinnik *et al.* 1998). The records were obtained at a number of stations in southeast Asia. We discuss the data for two events out of four.

The data for 1994 November 15 event (the deconvolved seismograms at nine stations, their stack and the stack of synthetic seismograms) are displayed in Fig. 5. The stack of the actual

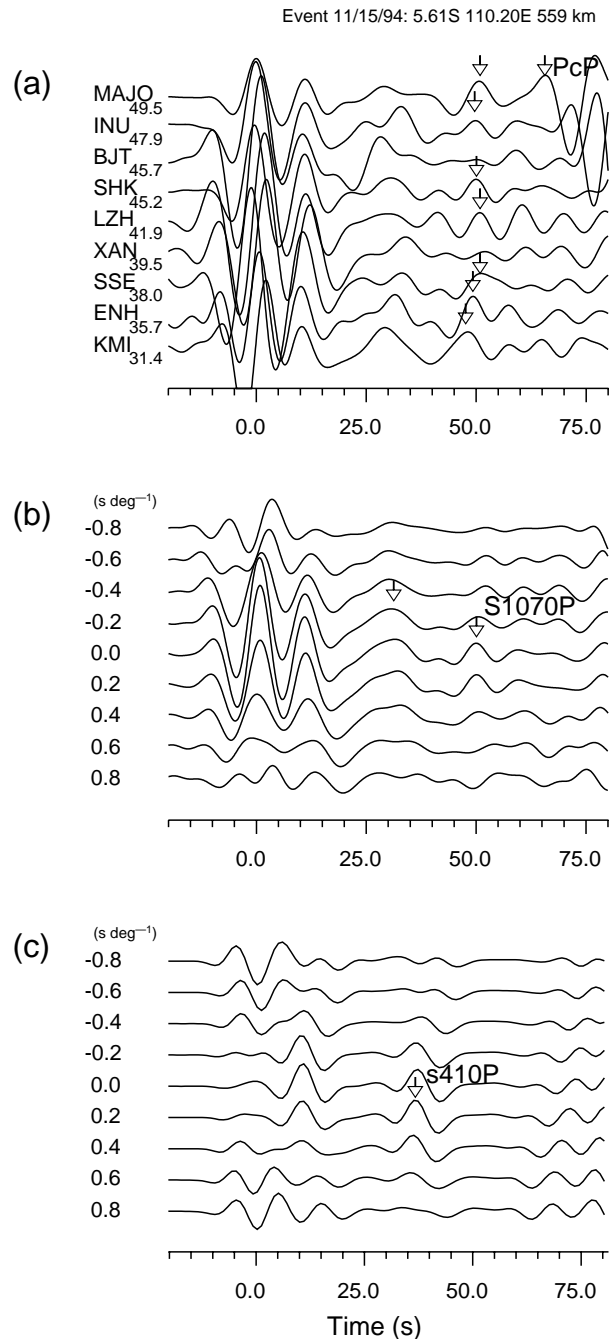


Figure 5. Data for the 1994 November 15 event; detected phases are marked by arrows. (a) Deconvolved vertical component traces; epicentral distances and station codes are shown on the left. (b) Stack of traces in (a); differential slowness is indicated on the left. (c) The same as (b) but for synthetics for IASP91.

recordings reveals two bumps: one with a time of 30 s and the other with a time of 50 s. The signal at 50 s was observed in short-period recordings of this event at the J-array in Japan (Niu & Kawakatsu 1997). Normalized amplitudes of both phases are around 0.015. The second phase can be recognized in most of the individual seismograms. The synthetic stack contains $s^{\prime}410^{\circ}P$ phase that arrives 14 s earlier than the second signal in the actual seismograms. 10 km in differential depth (between the focus of event and the reflector) is equivalent to 2.7 s in time, and the discrepancy between the times of $s^{\prime}410^{\circ}P$ phase and the signal at 50 s is too large to be explained by uncertainties in the event depth or/and the depth of the '410 km' discontinuity. The signal at 30 s also looks very different from $s^{\prime}410^{\circ}P$ phase.

The main P -wave group (at times less than 20 s) looks different in the stack of the synthetics and the actual data. This discrepancy is caused by locations of the stations close to the nodal line, where amplitudes of the P phase are unstable. This discrepancy is of minor significance for our analysis, and in most other cases considered it is not observed.

Interpretation of the data in Fig. 5 is simplified by comparing them with the data for the 1994 September 28 event in Fig. 6. Coordinates of the epicentres and the seismograph networks for the two events are almost the same, their focal mechanisms are similar, but the depths are strongly different (559 km and 643 km, see Table 1). The stack in Fig. 6 is shown

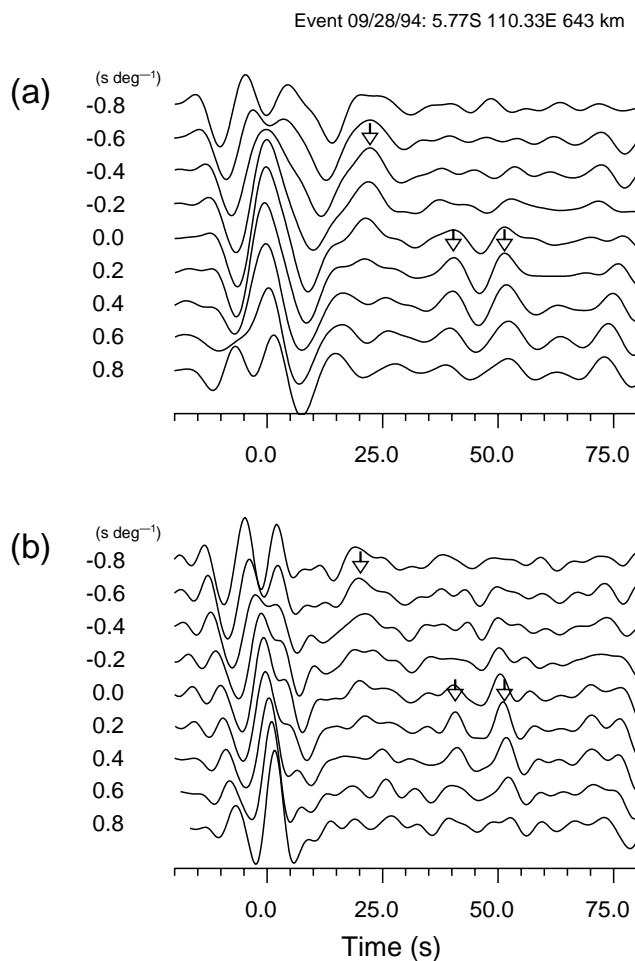


Figure 6. Data for the 1994 September 28 event; detected phases are marked by arrows. (a) Stack of deconvolved vertical component traces (7 stations). (b) The same as (a) but with a shorter-period filtering.

at the same period as in Fig. 5 and at a shorter period. In the longer-period stack two bumps with a positive polarity and a normalized amplitude of around 0.015 are seen at 40.4 s and 51.8 s. These two phases could be interpreted as side lobes of one phase with a negative polarity. However, the stack for shorter periods demonstrates that this is unlikely. The phase at a time around 40 s was observed in short-period records of this event at the J-array (Niu & Kawakatsu 1997). The slowness of both phases is positive (around 0.3 s deg^{-1}). Another bump, with a negative slowness is observed at a time around 20 s. This phase becomes very distinct at the shorter periods.

The SdP phase from the same discontinuity should arrive about 9 s earlier in Fig. 6 than in Fig. 5. Then the arrivals at a time around 30 s in Fig. 5 and at around 20 s in Fig. 6 can be interpreted as SdP phases from a discontinuity at a depth of 860 km. The arrivals at 50 s in Fig. 5 and at 40.4 s in Fig. 6 can be interpreted as SdP phase from a discontinuity at a depth of 1070 km. Positive slowness of the arrival with a time of 40.4 s in Fig. 6 contradicts this, but we don't see any alternative possibility. It is conceivable that the estimate of slowness is biased by a topography on the discontinuity; if the converting discontinuity has a topography on it, the recorded signal may propagate to some stations off the great circle and arrive several seconds later than from a horizontal interface at the same depth. The arrival at 51.8 s in Fig. 6 can be interpreted either as $s^{\prime}410^{\circ}P$ phase or as $S^{\prime}1170^{\circ}P$ phase or a superposition of both. Interpretation of this signal as $s^{\prime}410^{\circ}P$ is favoured by its time and slowness. However, a similar arrival seems to be present in the records of two other events (1992 September 2 and 1992 July 14), where it can not be interpreted as $s^{\prime}410^{\circ}P$ phase. Moreover, a similar positive slowness is displayed in Fig. 6 by the phase at a time of 40.4 s, which can hardly be interpreted as reflected in the source region.

A signal similar to that at 40.4 s in Fig. 6 was detected on broad-band seismograms of the 1992 September 2 event at stations in southeast Asia (Vinnik *et al.* 1998) and on short-period seismograms of the J-array (Niu & Kawakatsu 1997). The epicentre of this event is 2° east of the epicentres of the 1994 November 15 and 1994 September 28 events, the depth is close to that of the 1994 September 28 event, but the time of the signal is 6 s less. The time difference implies the presence of a strong topography on the discontinuity (the discontinuity is uplifted by 60 km). Another phase which arrives with a delay of 9 s relative the first can be $S^{\prime}1110^{\circ}P$. This phase arrives much earlier than $s^{\prime}410^{\circ}P$ phase (at 55 s). Finally, the SdP phases corresponding to '1070 km' and '1170 km' discontinuities were identified on the seismograms of the 1992 July 14 event, 15° east of the 1994 November 15 and 1994 September 28 events (Vinnik *et al.* 1998). The time of $s^{\prime}410^{\circ}P$ phase for the 1992 July 14 event is very small, and it could not be mistaken for either $S^{\prime}1070^{\circ}P$ or $S^{\prime}1170^{\circ}P$ phase.

Interpretation of the presented observations in terms of SdP phases can be tested further by comparing them with the data for event with a strongly different radiation pattern. Amplitudes of the parent SV for SdP phases of the 1998 May 23 event (8.1° N , 123.7° E , 657.8 km) are negligible, but for $s^{\prime}410^{\circ}P$ phase they are stronger by an order of magnitude. Fig. 7 shows the stack for 10 stations in the distance range between 26° and 48° and the stack of the related synthetics. In agreement with the focal mechanism the actual recordings contain no visible SdP phases in the time interval between 20 and 70 s. In the synthetics there is a strong $s^{\prime}410^{\circ}P$ signal, which is missing from

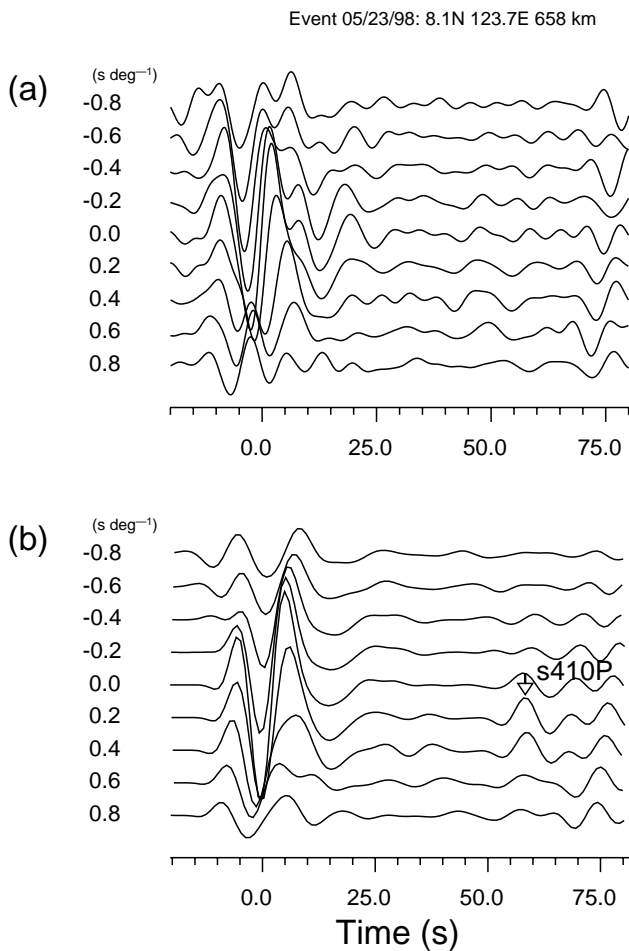


Figure 7. Stack of deconvolved vertical component traces for the event of 1998 May 23, 8.1 N (lat), 123.7 E (lon), 657.8 km (depth), with a weak radiation for SdP phases and a strong radiation for $s'410'P$ phase. (a) Actual recordings, (b) Synthetics for IASP91.

the actual seismograms. This phase is reflected from '410 km' discontinuity in the region outside the subducted slab. Therefore strong lateral variations of temperature and the related topography on '410 km' discontinuity can be ruled out as an explanation for the weakness of $s'410'P$ phase. It is possible that a similar wavefield without visible $s'410'P$ phase is present in the seismograms of the 1994 November 15 and 1994 September 28 events.

EVENTS IN THE KERMADEC-FIJI-TONGA REGION

Several deep events in the Kermadec-Fiji-Tonga region with a suitable radiation pattern were well recorded by the broadband stations in east Asia and a network in Japan. The radiation pattern of one event is demonstrated in Fig. 8. This pattern is broadly similar to those of the other events of this group. We will present the data starting from the southernmost 1997 March 21 event and then proceed to the north.

1997 March 21 event

The event was recorded by the J-array and FREESIA networks in Japan as well as by the stations in east Asia. The results of data processing are displayed in Fig. 9. Seismograms of 34 stations in Japan at epicentral distances between 76° and 83° were deconvolved by the SH waveform at station GUMO. A clear-cut signal with negative slowness appropriate for SdP phases, positive polarity and normalized amplitude of 0.01 is detected at a time of 61.5 s (Fig. 9a). This signal is not seen in the synthetics for standard model (Fig. 9b). A discontinuity with the S velocity contrast of 0.2 km s^{-1} was placed at a depth of 1200 km in the standard model. The stack of the related synthetic seismograms (Fig. 9c) contains the signal very similar to that in Fig. 9a.

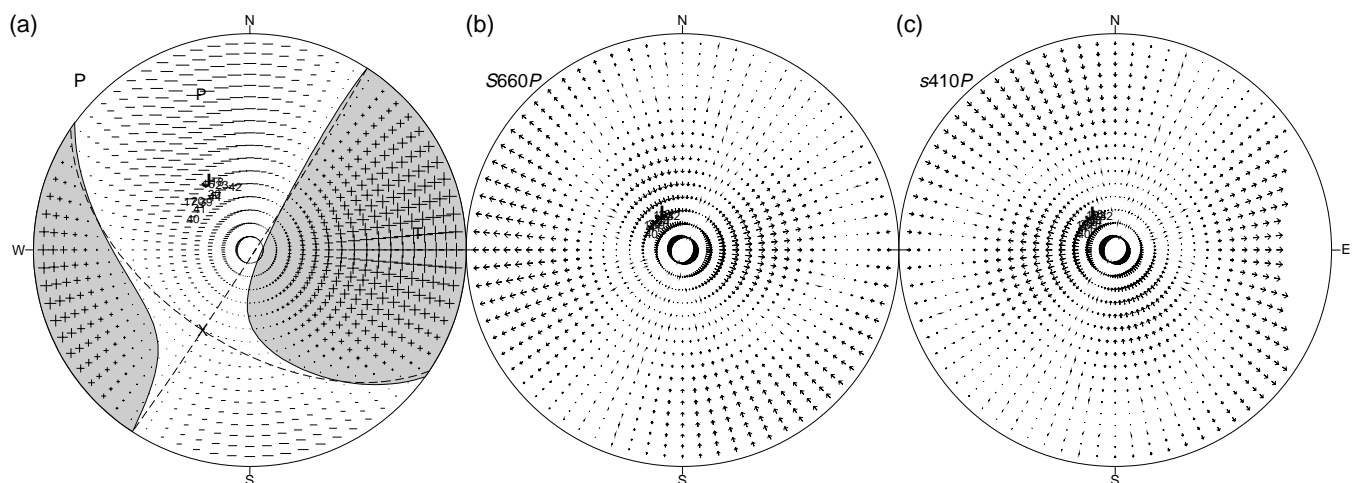


Figure 8. Theoretical amplitudes of P radiated downward (a) and SV radiated downward (b) and upward (c) for events in the Kermadec-Fiji-Tonga region. Each point of the Earth's surface is specified by its azimuth relative to the epicentre and the incidence angle in the source for P (a), $S'660'P$ (b) and $s'410'P$ (c). Seismograph stations are indicated by numbers: 16—MAJO, 17—TATO, 18—ERM, 20—SSE, 23—YSS, 30—MDJ, 39—BJT, 40—KMI, 41—XAN, 42—MA2, 44—HIA. J is J-array + FREESIA.

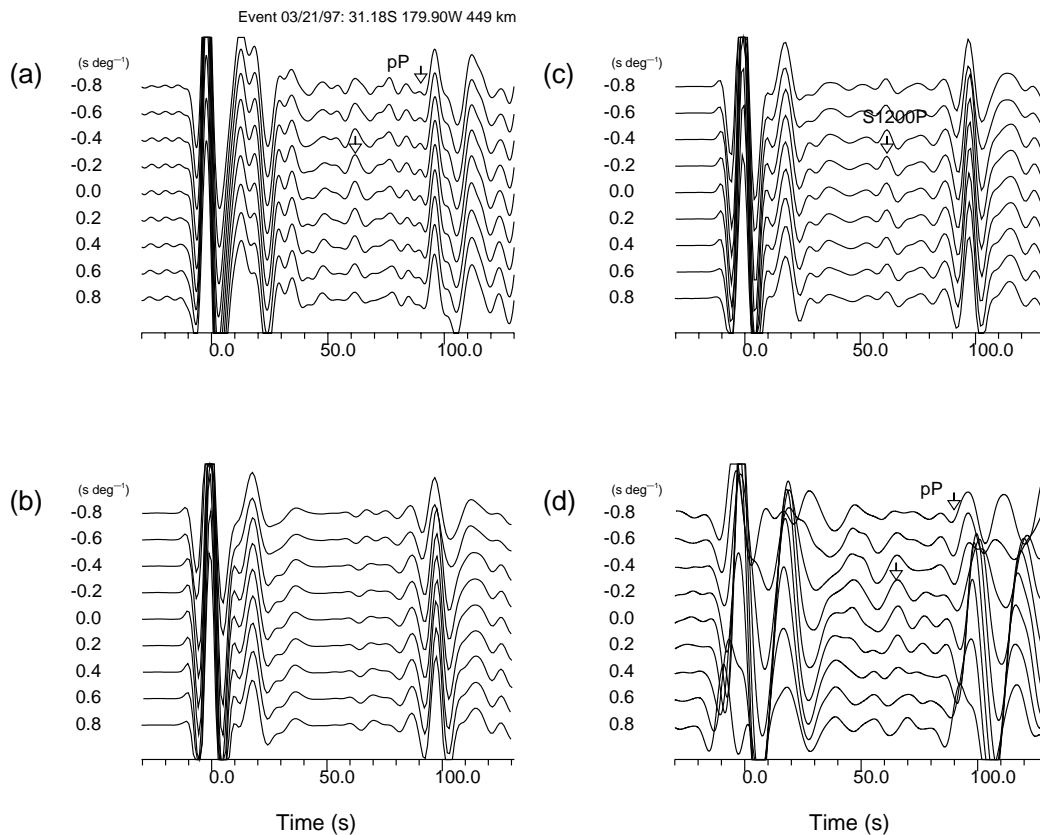


Figure 9. Data for the event of 1997 March 21; detected phases are marked by arrows. (a) stack of deconvolved vertical component traces of the J-array and FREESIA network. (b) The same as in (a) but for synthetics for IASP91. (c) The same as (b) but with a discontinuity at a depth of 1200 km; S velocity contrast at the discontinuity is 0.2 km/s. (d) The same as (a) but for stations in east Asia.

Seismograms of 11 stations in east Asia (MAJO, TATO, ERM, SSE, YSS, MDJ, BJT, KMI, XAN, MA2 and HIA) in the distance interval between 77.7° and 96.2° were deconvolved by the SH component of S phase at station GUMO. The stack of these seismograms (Fig. 9d) reveals the same signal as in Fig. 9a but delayed by 3.5 s. Like in Fig. 9a, its slowness is negative, appropriate for SdP phases. The depth of the discontinuity corresponding to the data in Fig. 9d is close to 1240 km.

The 1994 October 27 and 1997 September 4 events

The 1994 October 27 and 1997 September 4 events are located to the north of the 1997 March 21 event. The close spacing of these two events is complemented by a strong difference in depths (523 and 604 km, respectively). Seismograms of the 1994 October 27 event at 11 stations in east Asia in the distance interval between 79° and 96° were deconvolved by the SV component of S phase at station GUMO. Fig. 10 shows individual seismograms (a), their stack (b) and the stack of the respective synthetic seismograms (c). A signal with positive polarity is detected in the stack at a time of 55.5 s with a normalized amplitude of around 0.01. The signal is well seen at about half of the individual seismograms. At negative slowness this signal interferes destructively with a pulse of negative polarity. The time of the pulse with negative polarity changes with slowness, and its origin is unclear. Synthetic seismograms for standard model contain no signal in this time interval. If the signal at

55.5 s is SdP phase, the depth of the related discontinuity is around 1250 km, close to the depth of the discontinuity found from the similar data for the 1997 March 21 event.

The 1997 September 4 event is recorded by both the network in Japan (18 stations, most of them at distances $72\text{--}73^\circ$) and seismograph stations in east Asia. Seismograms of the J-array and FREESIA network in Japan are deconvolved by their respective SH components. The stack (Fig. 11a) contains a strong signal at a time around 50 s, which corresponds to $s'410^\circ P$ phase in the synthetics (Fig. 11b). Another noteworthy feature of the synthetics is a weak signal with negative polarity at a time of 90 s. This is $Pp'410^\circ P$ phase (P reflected from the Earth's surface and the '410 km' discontinuity in the receiver region, Fig. 4). In the actual recordings this phase is not seen.

The data for the same event recorded by 10 stations in east Asia (TATO, SSE, QIZ, MDJ, BJT, CHTO, KMI, XAN, HIA, LZH) in the epicentral distance interval between 75° and 94° are displayed in Fig. 12. The seismograms were deconvolved by the SH component of S phase at station GUMO at an epicentral distance of 51.5° . In the stack of these seismograms (Fig. 12a) there is a signal at 45.5 s with positive polarity and a normalized amplitude of 0.015. The theoretical waveform of $s'410^\circ P$ phase in the synthetics (Fig. 12b) is strongly different from the signal observed in the actual data. If the signal in Fig. 12(a) is SdP phase, the depth of the related discontinuity is 1210 km, close to that found from the records of the 1994 October 27 event. The $Pp'410^\circ P$ phase is seen in synthetics in Fig. 12(b), but not in the actual recordings in Fig. 12(a).

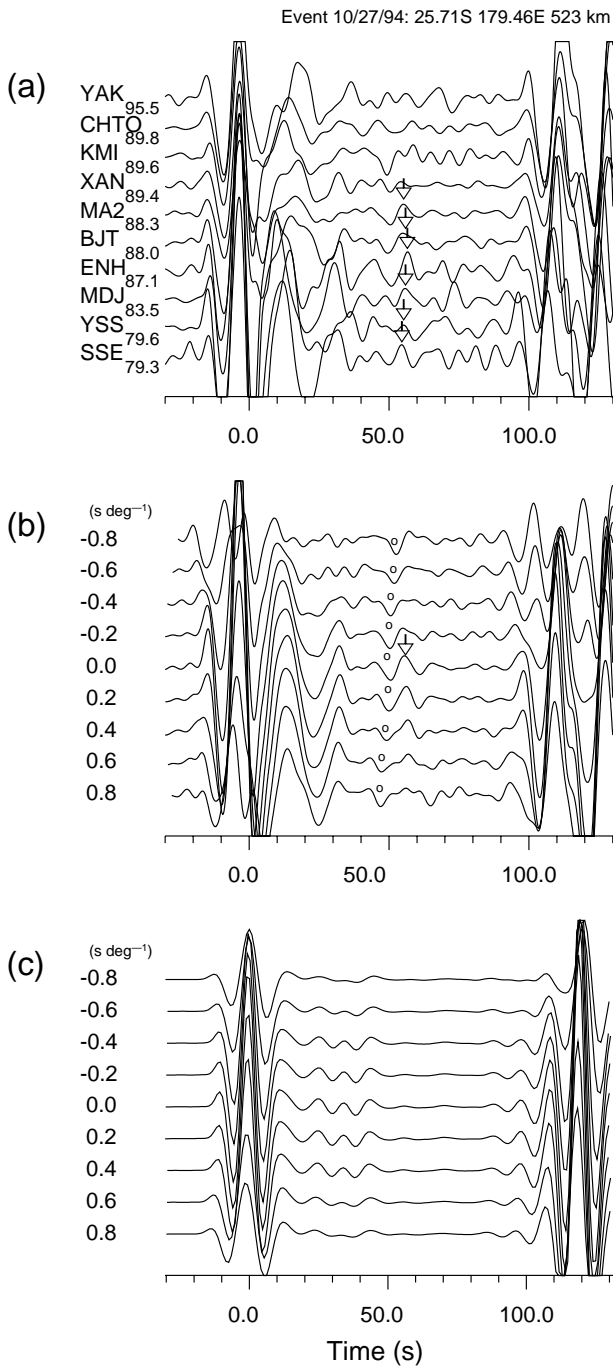


Figure 10. The same as in Fig. 5 but for the 1994 October 27 event. An arrival in (b) which interferes with the presumed *SdP* phase is marked by circles.

The 1998 May 16 and 1994 March 31 events

The 1998 May 16 and 1994 March 31 events are located further to the North, close to each other and at about the same depth. The 1998 May 16 event was recorded by both the network in Japan and the network in east Asia. Seismograms of 17 stations in east Asia in a distance interval between 71° and 96° (MAJO, ERM, TATO, YSS, PET, SSE, QIZ, MDJ, MA2, BJT, XAN, KMI, HIA, CHTO, BILL, YAK, ULN) were deconvolved by the *SH* component of the *S* phase at station

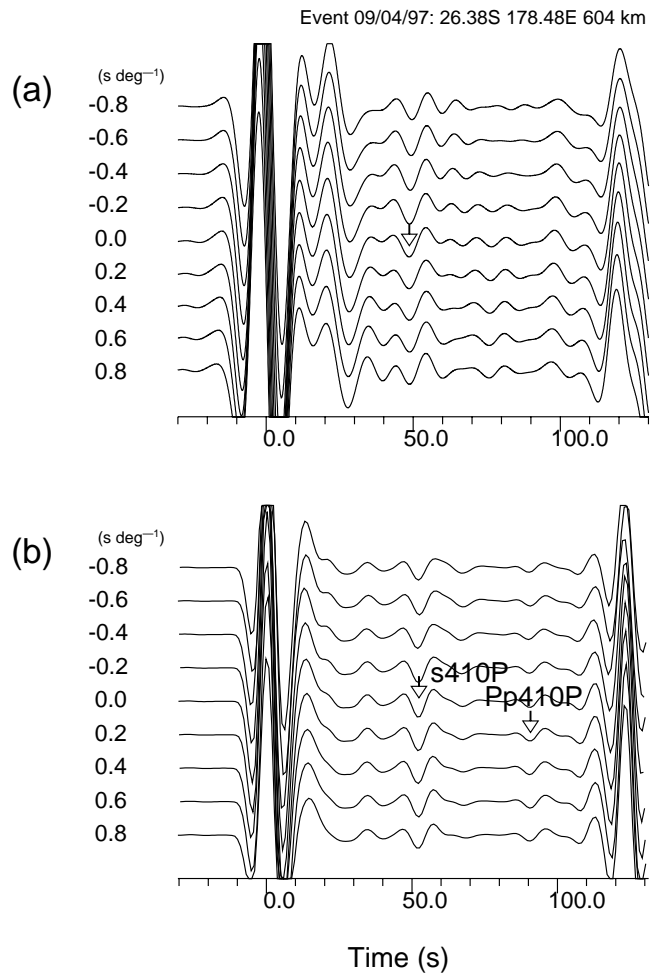


Figure 11. Data for the event of 1997 September 4 at the J-array and FREESIA; the detected phases are marked by arrows. (a) Stack of the deconvolved vertical component traces. (b) The same as in (a) but for synthetics for IASP91; phase at 90 s is *Pp*'410'*P*.

ERM in Japan at a distance of 72.6°. The stack of these seismograms (Fig. 13a) reveals a strong phase at a time around 50 s which looks similar to *s*'410'*P* phase in the synthetics (Fig. 13b). A weak signal in the synthetics at 90 s is the *Pp*'410'*P* phase. This phase is not seen in the actual seismograms, but a signal with opposite polarity arrives at 98 s. If this is *SdP* phase, the depth of the discontinuity is close to 1800 km. A similar wavefield was observed in the records of the J-array and FREESIA network in Japan.

The data for the nearby 1994 March 31 event are displayed in Fig. 14. Seismograms of 13 stations in east Asia (MAJO, TATO, YSS, SSE, QIZ, MDJ, ENH, BJI, XAN, KMI, HIA, CHTO, LZH) in the distance range between 70.5° and 92.5° were deconvolved by *SH* component of the *S* phase at MAJO. The stack of these seismograms reveals a phase with negative slowness and positive polarity at 42 s. Its waveform is strongly different from the waveform of *s*'410'*P* phase in synthetic seismograms. If it is *SdP* phase its normalized amplitude is around 0.02, and the depth of the related discontinuity is around 1120 km. *Pp*'410'*P* phase is seen at 90 s in the stack of synthetic seismograms. The pulse with positive polarity at 98 s in the actual recordings can be interpreted as *SdP* phase from a discontinuity at a depth of 1800 km.

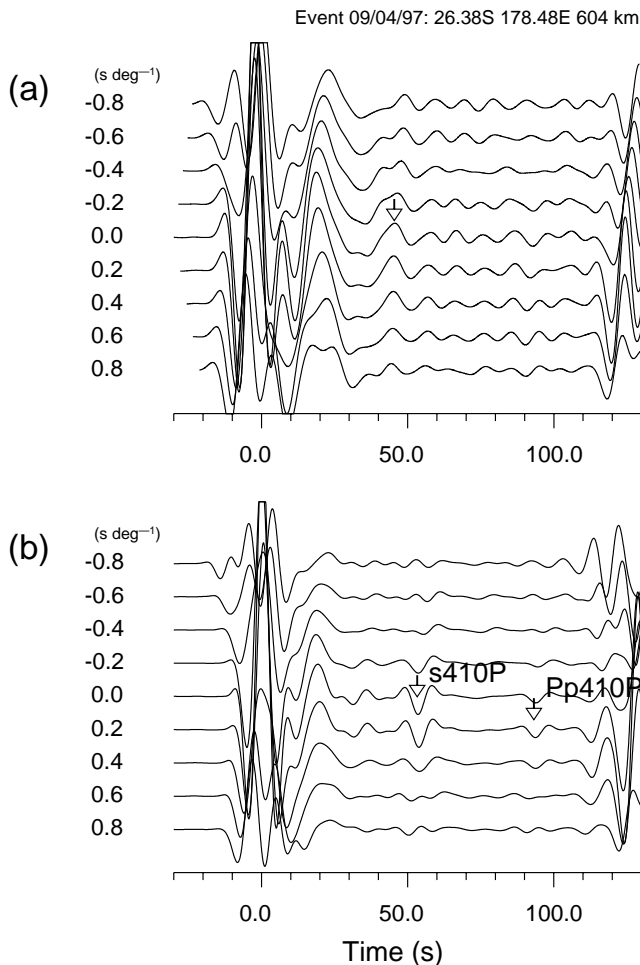


Figure 12. The same as in Fig. 11 but for stations in east Asia.

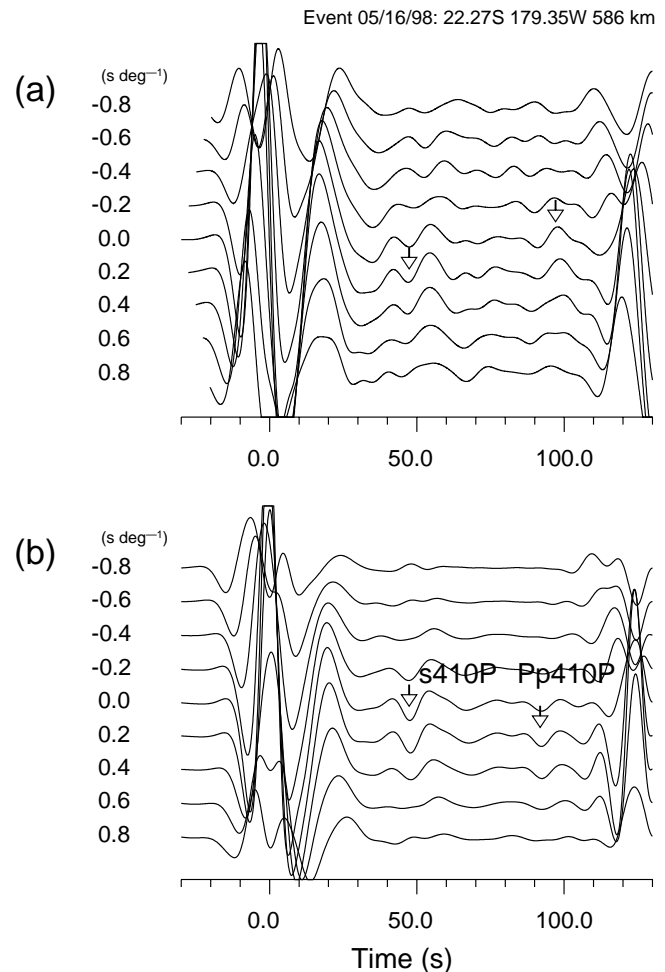


Figure 13. The same as in Fig. 12 but for the 1998 May 16 event.

The 1993 August 7 and 1998 March 29 events

The 1993 August 7 event occupies an intermediate position between the events of 1998 May 16 and 1997 September 4. Seismograms of 13 stations (MAJO, ERM, YSS, SSE, QIZ, MDJ, ENH, BJI, XAN, KMI, CHTO, HIA, LZH) in the distance interval between 71.8° and 93.2° are deconvolved by the SH component of S phase at station ERM. In the stack (Fig. 15), a signal-like feature is observed at 41 s, with a normalized amplitude of around 0.035. What leads us to believe that this is the SdP phase rather than reverberation in the source or/and receiver regions is its strong focusing at a negative slowness (-0.6 s deg^{-1}), contrary to the main P wavetrain which is focused at 0 s deg^{-1} . Negative slowness is appropriate for SdP phase. In the synthetic seismograms for standard model this feature is missing. If the arrival at 41 s is SdP phase, it is converted at a depth around 1050 km.

The 1998 March 29 event is in the far north of the region. The seismograms of 10 stations in the distance range between 71.6° and 90° (TATO, YSS, SSE, MDJ, MA2, BJT, ENH, XAN, HIA, LZH) were deconvolved by SH component of the S phase at station PET. The stack (Fig. 16) reveals a signal at a time of 44 s with an amplitude of around 0.02. The signal is seen mainly in the negative slowness range, in agreement with the theoretical slowness of SdP phases. The amplitude and waveform of this signal are very different from those of s^410P

phase in synthetic seismograms. If this is SdP phase, the depth of the related discontinuity is close to 1070 km. The stack in Fig. 16(a) is only one in actual data, where Pp^410P phase at 90 s is seen reasonably clearly as a pulse of negative polarity at the traces corresponding to 0.6 and 0.8 s deg^{-1} . In the stack of 42 seismograms of this event at the J-array and FREESIA network in the distance interval between 65° and 71.5° (not shown in Fig. 16) the signal at 44 s cannot be seen, because at these relatively small distances the seismograms are contaminated by PcP arrivals.

EVENTS IN THE NORTHWEST PACIFIC

Several deep events in the Mariana, Izu-Bonin and Japan subduction zones with appropriate radiation patterns were well recorded by stations in the west of North America.

The 1994 July 21 and 1999 April 8 events

The 1994 July 21 and 1999 April 8 events in the China–Russia border region are located close to each other but at very different depths (473 and 563 km, respectively). Seismograms of the former event at 26 stations at distances from 68.4° to 88.8° were deconvolved by the SV component of S phase at station COR at an epicentral distance of 70° . The stack (Fig. 17) reveals a strong phase with positive polarity at a time of 60.1 s,

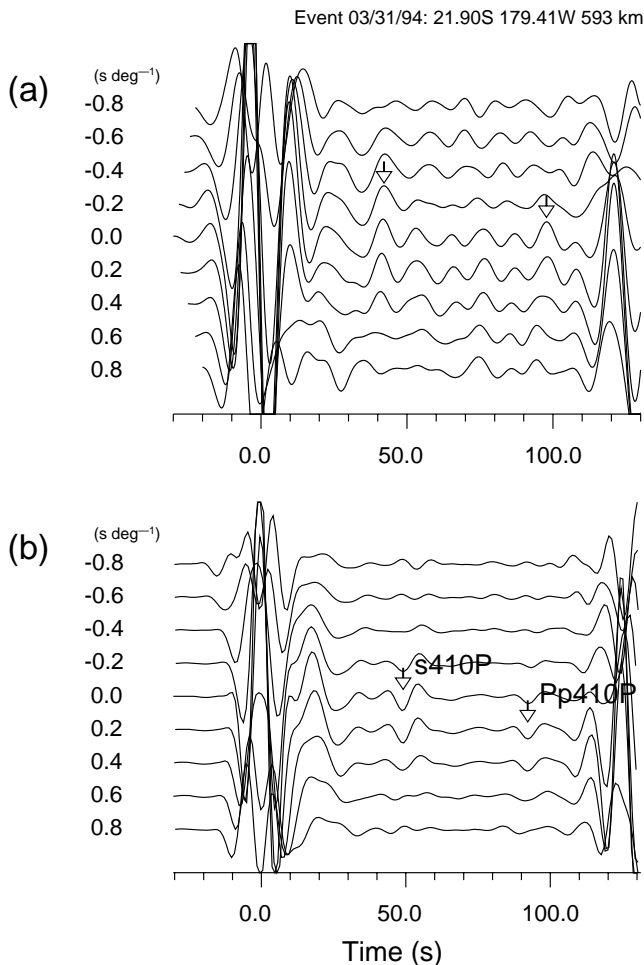


Figure 14. The same as in Fig. 12 but for the 1994 March 31 event.

which is focused at a slowness of -0.2 s deg^{-1} , appropriate for *SdP* phases. Its normalized amplitude is 0.027. This phase is followed by a weaker phase with positive polarity and a negative slowness at a time of 72.4 s. The first pulse is clearly seen in the traces obtained by summing 5–6 seismograms of neighbouring stations (Fig. 17b). Between these two arrivals there is a pulse of negative polarity, which is focused at a positive slowness. Interpretation of any of the detected signals as *s'410'P* phase is ruled out, because it arrives a few tens of seconds earlier, and the stack of synthetic seismograms for standard model contains no visible phases in the time window of interest. This leaves the *SdP* phases as the most likely possibility for interpreting the arrivals with positive polarity. For signals at 67.2 s and 72.4 s the depths of the discontinuities are 1200 km and 1340 km. The pulse with negative polarity and a positive slowness could be formed by reverberation in the source region.

For the 1999 April 8 event, 74 seismograms, almost all of them at epicentral distances between 67° and 83° , were deconvolved by the *SH* component of *S* phase at station LLLB at an epicentral distance of 67.1° . In the stack (Fig. 18a) two phases with normalized amplitudes of around 0.01 are detected at 51.0 and 70.0 s. Both are focused at a negative slowness appropriate for *SdP* phases. In synthetic seismograms *s'410'P* phase with negative polarity arrives at 42 s, and its positively polarized

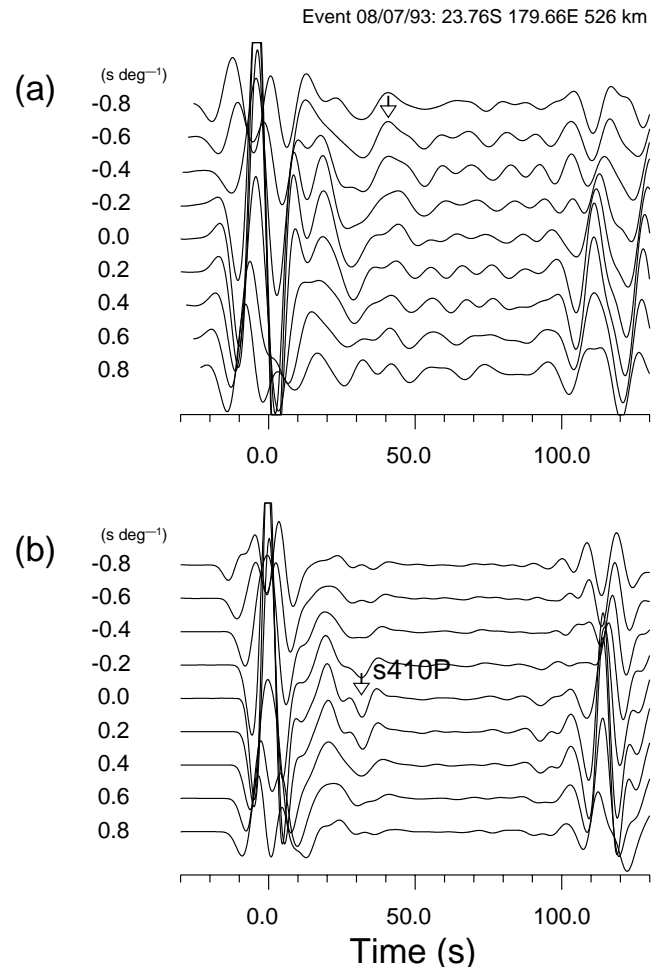


Figure 15. The same as in Fig. 12 but for the 1993 August 7 event.

sidelobe is seen at 46 s. This sidelobe could contribute to the amplitude of the signal at 51.0 s. However, the actual *s'410'P* phase should be much weaker than in the synthetics, because it is reflected within the subducted plate and its nearest vicinity (see Fig. 1). The reflectivity of the '410 km' discontinuity in this zone is so low, that even the *P'410's* converted phase could not be detected in this region with a local network of several stations (Vinnik *et al.* 1996). Therefore the signal at 51 s should be interpreted as *SdP* rather than *s'410'P* phase. The depth of the related discontinuity is 1200 km, equal to that found for the 1994 July 21 event. The same depth of the discontinuity suggests that this indeed is *SdP* phase from a discontinuity at 1200 km depth. The second phase is in the time interval, where no arrivals of comparable strength are seen in synthetic seismograms. If this is *SdP* phase, the related discontinuity is at a depth of 1430 km, much deeper than inferred from the data of the 1994 July 21 event, and the proposed interpretation remains unconfirmed.

The 1995 August 23 and 1995 August 24 events

This group consists of the main event in the Mariana subduction zone and its largest aftershock. Kaneshima & Helffrich (1998) relocated this sequence of deep earthquakes with the joint hypocentre determination (JHD) technique, and found that

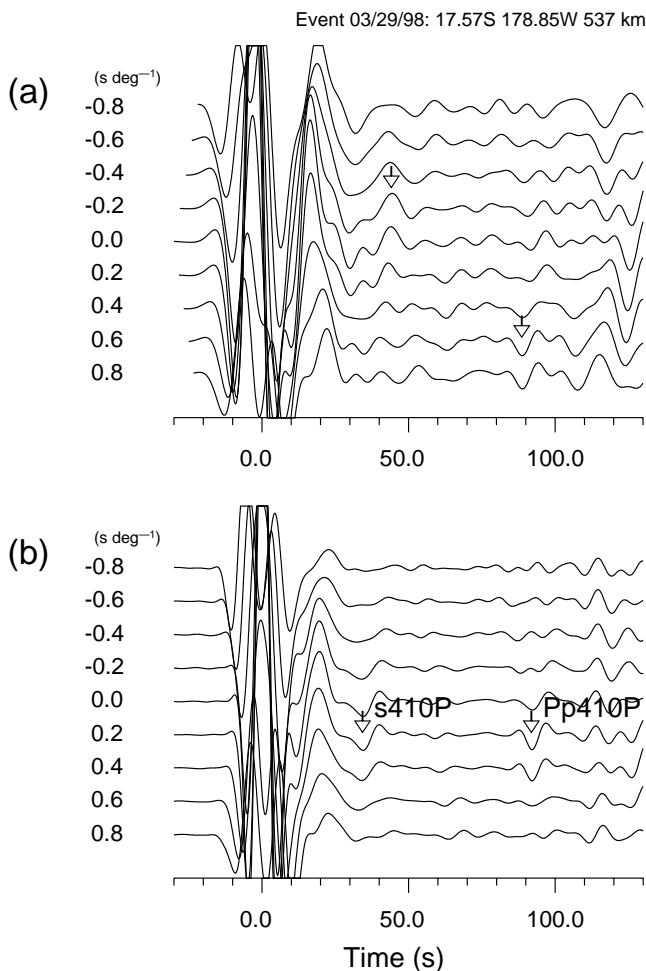


Figure 16. The same as in Fig. 12 but for the 1998 March 29 event.

the aftershock is deeper than the main event by 10 km. However, our analysis of various secondary phases suggests that the depths of both events are very similar. Focal mechanisms and the related radiation patterns for the two events are similar, as well. All stations, except COL and TUC are located in the epicentral distance interval between 78° and 87°. The seismograms of both events were deconvolved by the SH component of S phase at station COL, at a distance around 63°. Data for the first event are shown in Fig. 19. Similar results were obtained for the second event.

The stack of 36 seismograms of the 1995 August 23 event (Fig. 19a) demonstrates a number of phases, well correlated between the traces. Only two of them, at 51 and 88 s are left, when a stronger low-pass filtering is applied (Fig. 19b). Their normalized amplitudes are around 0.015. As demonstrated by synthetic seismograms for standard model (Fig. 19c), the signal at 51 s can be interpreted as $s^{\prime}410^{\circ}P$ phase, but the arrival at 88 s has no counterpart in the synthetics. This arrival is clearly a long-period component of the short-period (1–2 s) phase, which was observed by Wicks & Weber (1996) in the array recordings of deep Mariana events in California and interpreted as reflected from a fossil subduction zone. Kaneshima & Helffrich (1998) found that the travel time of this phase decreases with increasing event depth, which is indicative of SdP phase. The depth of the related discontinuity (assumed to be horizontal) is 1670 km.

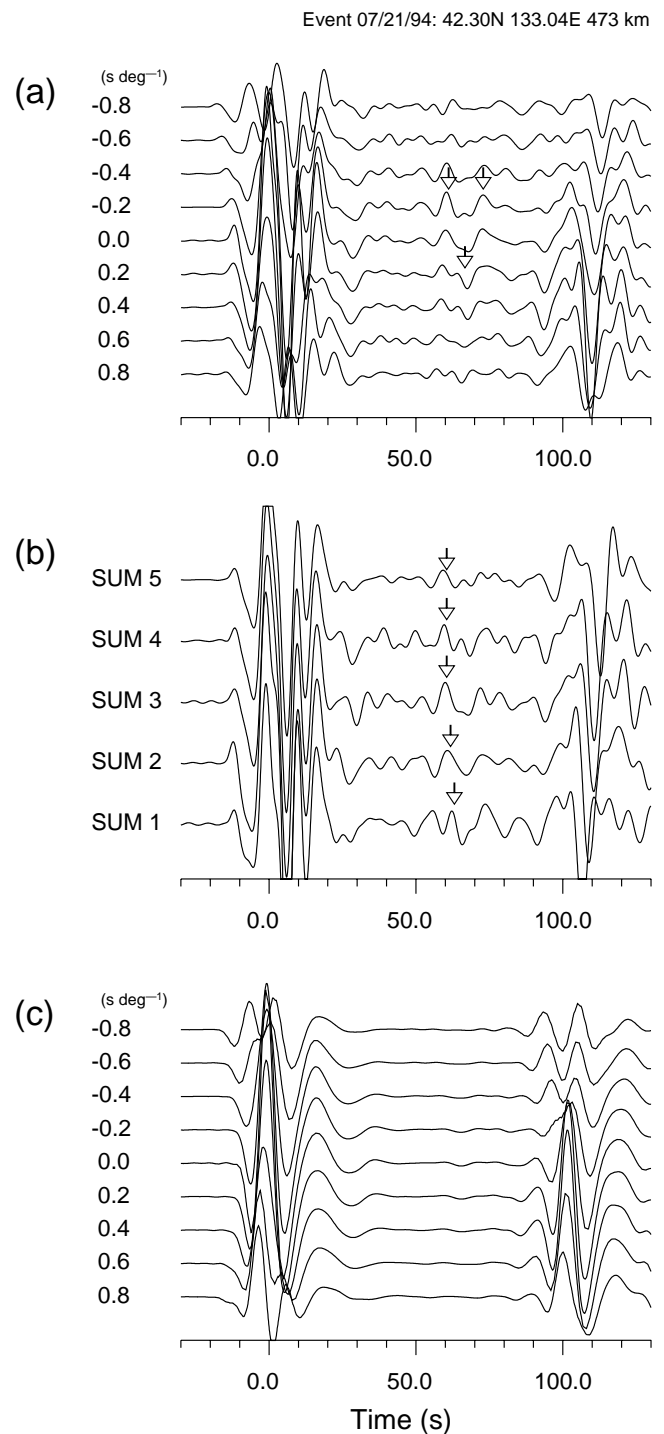


Figure 17. Data for the 1994 July 21 event; detected phases are shown by arrows. (a) Stack of deconvolved vertical component traces at stations in north America. (b) Summary traces obtained by summing 5–6 individual traces at neighbouring stations. (c) The same as in (a) but for synthetics for IASP91.

The 1996 March 16 and 1996 June 26 events

These two events in the Izu-Bonin region are located reasonably close. The 1996 March 16 event is well recorded by 40 stations in North America, almost all of them in the distance interval between 68° and 86°. The seismograms are deconvolved by the SV component of S phase at station COL at a

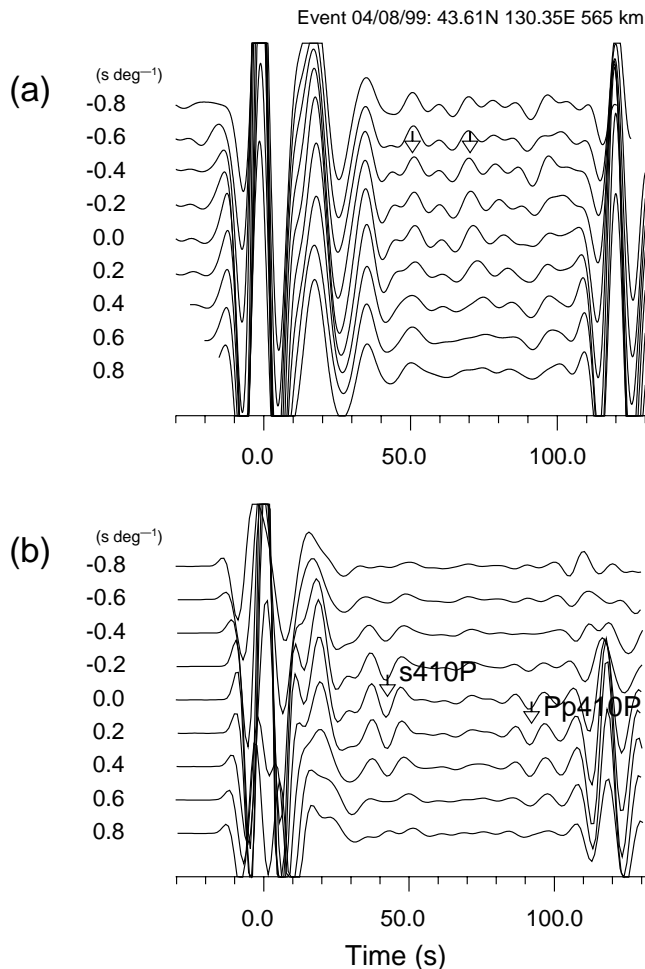


Figure 18. The same as in Fig. 12 but for the 1999 April 8 event and stations in north America.

distance of 57.1° . In the stack (Fig. 20a) there is a phase at a time of 34.0 s with a normalized amplitude of around 0.01. For the 1996 June 26 event, 45 seismograms were deconvolved by the *SH* component of *S* phase at station WHY. The stack (Fig. 20b) reveals the same phase with the same amplitude at a time of 32.8 s. Whereas epicentral distances of most stations for the two events differ by only 0.2° , *pP* phase of the 1996 June 26 event arrives 2 s later relative to *P*. This difference suggests that the event of 1996 June 26 is about 10 km deeper than the other event. Then a smaller time of the signal on the seismograms of the 1996 June 26 event (32.8 s) relative to the other event (34.0 s) suggests that this is *SdP* phase, converted at the same depth. Synthetics for standard model (Figs 20c and d) don't contain strong phases in this time interval. If the phase in the seismograms of the events of 1996 March 16 and 1996 June 26 is *SdP*, the depth of the related discontinuity is around 880 km.

DISCUSSION

We have inspected all digital recordings of deep events that were available at the end of 1999. Many seismograms appeared to be unsuitable for our purpose for such reasons as unfavourable radiation pattern, strong noise or too few broad-band stations in the distance range of interest. In spite of this we got several reliable results. The clearest *SdP* phases (events 1997

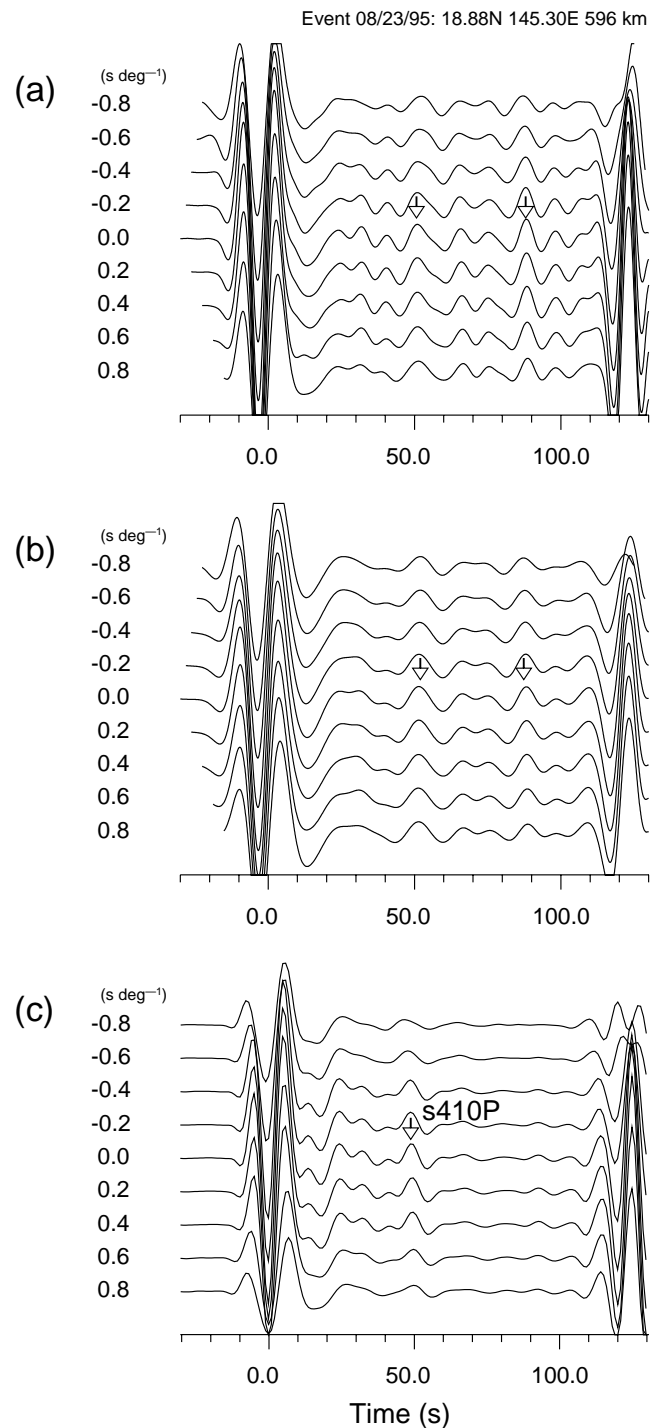


Figure 19. Data for the 1995 August 23 event. (a) Stack of deconvolved vertical component traces at stations in north America. (b) The same as in (a) but with a longer-period filtering. (c) The same as in (a) but for synthetics for IASP91.

March 21 and 1994 July 21, Figs 9 and 17) correspond to the '1200 km' discontinuity at the south of the Kermadec–Fiji–Tonga region and to the west of Japan, respectively. In both cases the signal is much stronger than noise and is focused at a negative slowness, appropriate for *SdP* phases. In synthetic seismograms for standard model there are no phases of comparable strength in the time window of interest. A signal similar to that from the 1997 March 21 event is seen in the records of

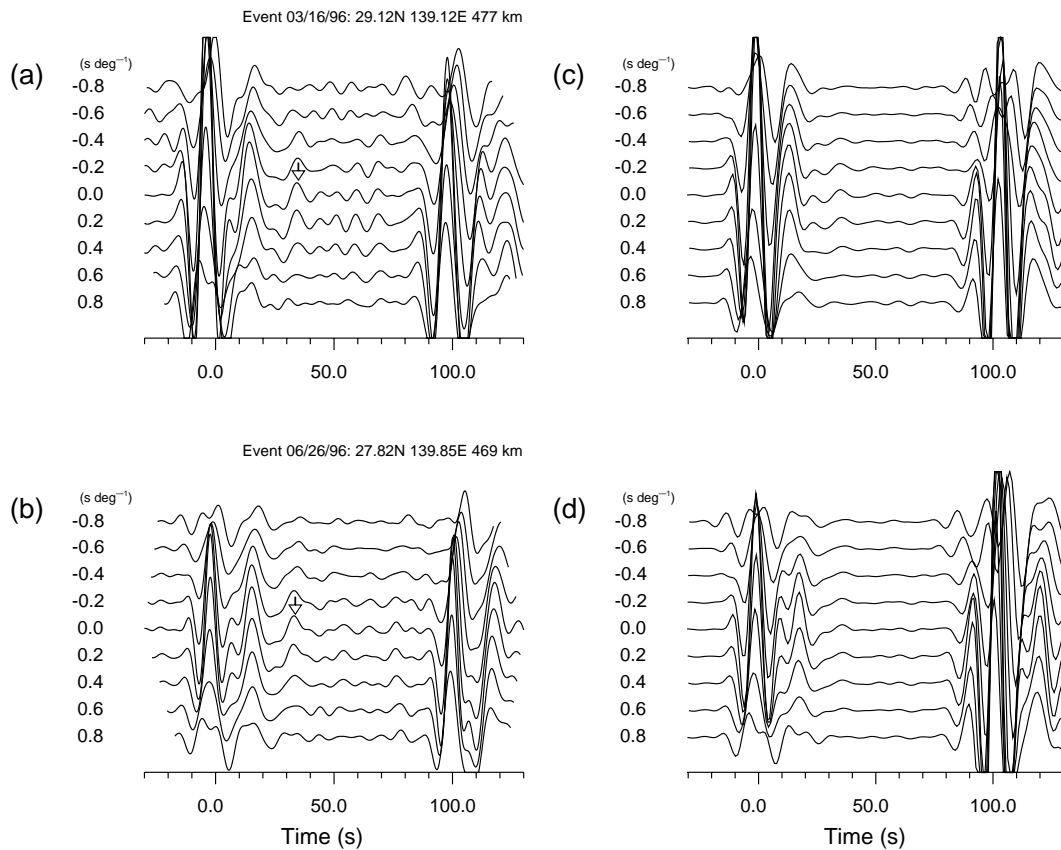


Figure 20. Data for the 1996 March 16 and 1996 June 26 events. (a) Stack of deconvolved vertical component traces of the 1996 March 16 event at stations in North America. (b) The same as in (a) but for the 1996 June 26 event. (c) The same as in (a,b) but for synthetics for IASP91.

the 1994 October 27 event (Fig. 10), a few degrees to the north. This interpretation is further supported by the data for the 1997 September 4 event (Fig. 11) which occurred in about the same location as the event of 1994 October 27 but at a different depth. Interpretation of the signal in the records of the 1994 July 21 event as $S^{1200}P$ phase is confirmed by the observation of a similar phase in the records of the 1999 April 8 (Fig. 18) at a strongly different depth.

The other data that can be included in the group of the most reliable are SdP phases from the discontinuity at a depth of 860–880 km. These phases are found in recordings of the 1994 November 15 and 1994 September 28 events in the Sunda arc region (Figs 5 and 6) and the 1996 March 16 and 1996 June 26 events in the Izu-Bonin region (Fig. 20). The signal in these records is focused at a slowness appropriate for SdP phases, and similar arrivals are absent from synthetics for standard model. Arrival times in the records of events at different depths confirm this interpretation.

Observation of SdP phase from a discontinuity at a depth of 1670 km in the Mariana islands region (events 1995 August 23, Fig. 19, and 1995 August 24) belongs to the most reliable group, as well. Kaneshima & Helffrich (1999) reported that this phase is converted from a dipping low-velocity layer, which presents a former oceanic crust at the top of a subducted plate. We find this unlikely. Our data show that the signal comes from a discontinuity with a positive S velocity contrast of around 0.3 km s^{-1} . Whereas the subducted plate model can not be reconciled with any other geophysical or geochemical data, the discontinuity in this depth range was found many times, starting

from Geiger & Gutenberg (1912). Evidence of a strong discontinuity in about the same region and at about the same depth can be seen in the results of direct P -wave slowness measurements at the Kamchatka network (Vinnik & Slavina 1975). The signal from a depth of 1800 km (events on 1998 May 16 and 1994 March 31 in the Fiji–Tonga region, Figs 13 and 14) may correspond to the same discontinuity, but this observation is less reliable, because both events are at the same depth.

The observations of SdP phase from a depth of 1070 km in the Sunda arc region may also be included in the group of the most reliable, although slowness of the signal in these records tends to be positive, instead of the negative, appropriate for SdP phases. This interpretation is strongly supported by the data for the 1994 November 15 and 1994 September 28 events (Figs 5 and 6), where the same signal arrives earlier in the records of the deeper event. Positive slowness can be attributed to a small number of stations and to a topography on the discontinuity. The topography is manifested by the significant deviation of depth of the discontinuity inferred from the records of the 1992 September 2 event. Similar travel times were obtained for this discontinuity from short-period recordings of the J -array by Niu & Kawakatsu (1997). However, the longer-period data do not support their assumption of ‘1070 km’ discontinuity and ‘900 km’ discontinuity being the same discontinuity with a strongly variable depth.

All other observations should be rated less reliable. For example, observations of phases presumably converted at 1050–1120 km depth in the north of the Kermadec–Fiji–Tonga zone (1994 March 31, 1993 August 7 and 1998 March 29,

Figs 14–16) are less reliable, because they could not be confirmed by the data for events at differing depths. New events may enable us to do this in the future. All observations are summarized in Fig. 21, where we classify the data into the reliable and less reliable ones. Boot-strap testing with available waveforms indicates that the signal level of those reliable *SdP* phases is above two standard deviations of the noise level.

The smallest normalized amplitude of *SdP* phases that can be detected with our technique is around 0.01. The corresponding *S* velocity contrast at the discontinuity is around 0.2 km s^{-1} or 3 per cent, but focusing/defocusing effects don't allow to relate the observed amplitude and the *S* velocity contrast accurately. *SdP* phases from '1200 km' discontinuity are detected with confidence in the records of 4 events (Fig. 21). In some other records a reliable detection is prevented by the presence of other phases, and there are 5 events where a detectable signal from this discontinuity is missing: 1994 November 15 (Sunda arc), 1993 August 7, 1998 March 29 (Fiji–Tonga), and 1996 March 16, 1996 June 26 (Izu–Bonin). *SdP* phases from the discontinuity at a depth of 860–880 km are detected reliably in the records of 4 events, and there are 2 events where these phases are missing: 1992 July 14 (Sunda arc) and 1994 July 21 (China–Russia border). The signal from the discontinuity at a depth of 1670 km is detected with confidence in the records of two events at the same location. At epicentral distances of 30° – 50° (events in the Sunda arc) this depth range is inaccessible. In the other records this signal can only be detected, if the event depth is more than about 550 km. But then this signal can interfere destructively with *Pp410P* phase. This may explain why we got so few data for this discontinuity. The signal from the discontinuity at a depth around 1100 km is detected reliably in the records of 4 events in the Sunda arc region, and it is missing in the records of events 1994 October 27 (Fiji–Tonga), and all events in the northwest Pacific. On the average, the ratio between the numbers of detected and missing signals is around unity, which suggests that the presence of detectable signals from the lower-mantle discontinuities is not a rare event.

The discontinuities at depths around 900, 1200 and 1700 km were previously found not only close to the presently active subduction zones, as in the present study, but also in a completely different environment. For example, the '1200 km' discontinuity was found in east Asia (Vinnik & Nikolayev 1970) and southern Africa (le Stunff *et al.* 1995). It is possible that these discontinuities are global, though laterally variable. Lateral variability is especially pronounced in the '900 km' discontinuity, the depth of which in different reports varies between about 800 and 950 km. Part of this scatter can be caused by errors of identification. Little is known about the discontinuity in the 1010–1120 km depth range outside the Sunda arc and Fiji–Tonga regions, and its global extent is questionable. Analyses of the *P*-wave traveltimes data often reveal discontinuities at a depth of around 2000 km and deeper. This depth range, however, can not be explored with our technique.

Possibilities for explaining the lower mantle discontinuities were discussed in the literature. According to Bina (1998), both (Mg,Fe)SiO₃ and CaSiO₃ perovskites may undergo structural distortion in the lower mantle. Complexities in the upper layer of the lower mantle can be caused by a downward extension of the garnet stability field or by stability of silicate ilmenite or by dissolution of aluminum and ferric iron into perovskite. Le Stunff *et al.* (1995) mention volatiles as a possible source of the complexities. The discontinuity at a depth around 1700 km can be related to the phase transformation of FeO to NiAs structure (Mao *et al.* 1996). High pressure transformations may also occur in (Mg,Fe)O (Bina 1998). The discontinuity at 1200 km depth can be related to the transformation of SiO₂ from stishovite to CaCl₂ structure (Tsuchida & Yagi 1989; Kingma *et al.* 1995). Basalt in lower mantle conditions transforms into the perovskite assemblage, with about 10–20 per cent stishovite (Kesson *et al.* 1994; Hirose *et al.* 1999). The content of stishovite may depend on the content of FeO (Fei *et al.* 1996): if the maximum solubility of FeSiO₃ in (Mg,Fe)SiO₃ perovskite is exceeded, mixed oxides may appear instead. Calculations by Karki *et al.* (1997) show that the transition in

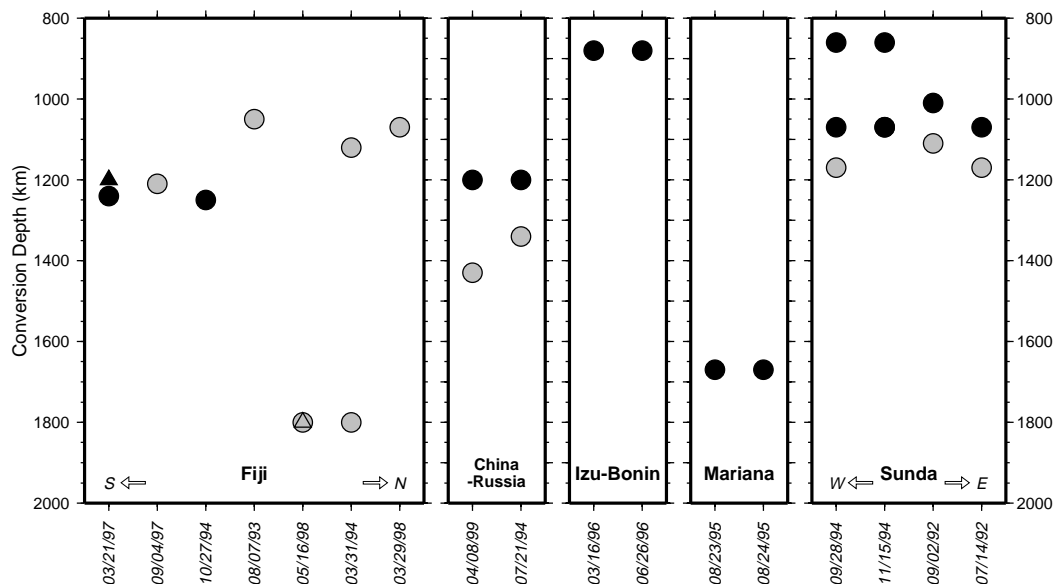


Figure 21. Summary of observations. Black and gray symbols are for the reliable and less reliable data. Data from the J-array and FREESIA are shown by triangles.

SiO₂ results in a sharp increase of the *S* velocity with depth, which is preceded by a decrease over several tens of kilometres. The decrease would result in a downward motion in the corresponding *SdP* pulse, but this is not seen in our data. To reconcile the observed strength of '1200 km' discontinuity with the data of Karki *et al.* (1997) the required amount of SiO₂ is of the order of several per cent. Some other phase transformations in the lower mantle were reviewed by Pushcharovskii & Pushcharovskii (1998).

Tomographic images of the mantle have shown that the correlation between lateral velocity variations in different layers becomes very low at a depth of around 1000 km (Tanimoto 1990; Montagner 1994). This was confirmed by a few other studies and interpreted as indication of a barrier for convective flow. Detailed studies have shown that in this depth range some subducted slabs tend to stagnate (for a review see Fukao *et al.* 2001). Tomographic images of mantle discontinuities can be mistaken for images of flat lying slabs (Oreshin *et al.* 1998), but this seems unlikely for most subduction zones. Beneath the Sunda arc tomographic models indicate accumulation of a high-velocity material just above the mid-mantle discontinuity at 1070–1080 km depth (Niu & Kawakatsu, 1997). Apparently, the discontinuity may act as a barrier for subduction. In tomographic models of the Kermadec–Fiji–Tonga region the subducted slab flattens at a depth less than 1000 km in the north, but penetrates to a deeper layer in the south. Stratification of the lower mantle, as shown by our data, is also different in the south and the north. The dominant feature in the north is the discontinuity at a depth of 1050–1120 km, which was not detected in the south. Here again this discontinuity may act as a barrier for subduction.

There is a first-order difference between the patterns of subduction near the western and eastern margins of the Pacific; in the west, subducted slabs tend to stagnate at depth less than about 1200 km (Fukao *et al.* 2001), whereas in the east the Farallon slab is sinking deeply through the lower mantle (Grand 1994; Grand *et al.* 1997). A difference between these regions has also been noted long ago in the patterns of stratification of the lower mantle (Vinnik *et al.* 1972). Fig. 22 shows the results of direct measurements of *dt/dΔ* of the teleseismic *P* waves at large-aperture arrays in central Asia (top, after Vinnik & Nikolayev 1970) and north America (bottom, after Johnson 1969). The rough data for southeast Asia suggest strong and sharp changes in *dt/dΔ* at distances around 37° and 52°. These changes remain visible in the smoothing curve. The related discontinuities are at depths of about 900 and 1200 km. In spite of smoothing, the '1200 km' discontinuity seems to be much stronger in southeast Asia than in America, and the related difference in composition could affect the balance of torque acting on the slabs.

ACKNOWLEDGMENTS

We wish to thank the J-array, FREESIA, Northern California, Southern California, OHP DMC, IRIS DMC and Geoscope data centers for providing the research community with high-quality digital seismic data. The records were processed with the aid of Seismic Handler written by Klaus Stammler. The help by Fenglin Niu is appreciated. The GMT software package, freely distributed by Wessel & Smith (1995), was used in this study. The study has been conducted during the visit of one of

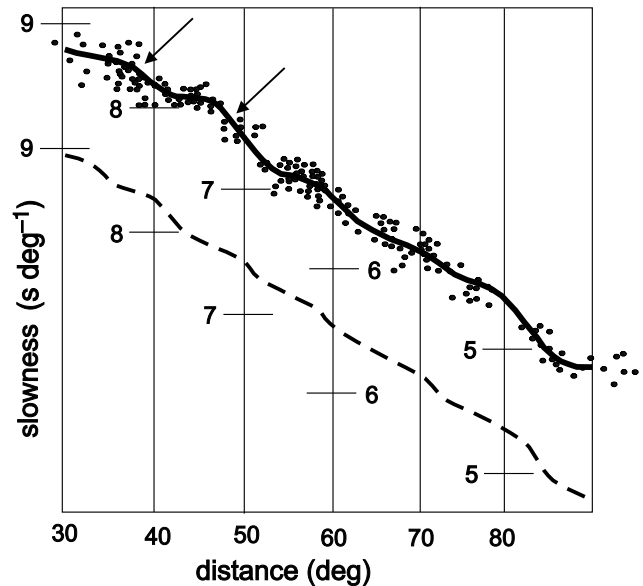


Figure 22. Results of direct measurements of *dt/dΔ* for the *P* waves at large-aperture arrays in central Asia [top, after Vinnik & Nikolayev (1970)] and in north America [bottom, after Johnson (1969)]. Measurements at arrays in the Tien Shan and south Siberia are shown by open and filled circles, respectively; sharp changes in *dt/dΔ* are marked by arrows.

the authors (LV) to the Earthquake Research Institute, and he thanks the Japanese colleagues for their hospitality. Partial support of LV by RFBR grant 98-05-64894 is acknowledged. Two anonymous reviews helped to improve the initial version.

REFERENCES

- Aki, K. & Richards, P., 1980. *Quantitative Seismology: Theory and Methods*, W.H. Freeman, San Francisco.
- Barley, B.J., Hudson, J.A. & Douglas, A., 1982. *S* to *P* scattering at the 650 km discontinuity, *Geophys. J. R. astr. Soc.*, **49**, 773–777.
- Bina, C.R., 1998. Lower mantle mineralogy and the geophysical perspective, *Rev. Mineral.*, **37**, 205–239.
- Bock, G. & Ha, J., 1984. Short-period S-P conversion in the mantle at a depth near 700 km, *Geophys. J. R. astr. Soc.*, **77**, 593–615.
- Castle, J.C. & Creager, K.C., 1999. A steeply dipping discontinuity in the lower mantle beneath Izu-Bonin, *J. geophys. Res.*, **104**, 7279–7292.
- Chinnery, M.A., 1969. Velocity anomalies in the lower mantle, *Phys. Earth planet. Inter.*, **2**, 1–10.
- Corbishley, D.J., 1970. Multiple array measurements of the *P*-wave travel-time derivative, *Geophys. J. R. astr. Soc.*, **19**, 1–14.
- Engdahl, R.E., van der Hilst, R. & Buland, R., 1998. Global teleseismic earthquake relocation with improved travel times and procedures for depth determination, *Bull. seism. Soc. Am.*, **88**, 722–743.
- Fei, Y., Wang, Y., Finger, L.W., 1996. Maximum solubility of FeO in (Mg, FeSiO₃-perovskite) as a function of temperature at 26 GPa: Implication for FeO content in the lower mantle, *J. geophys. Res.*, **101**, 11 525–11 530.
- Fuchs, K. & Mueller, G., 1971. Computation of synthetic seismograms with the reflectivity method and comparison with observations, *Geophys. J. R. astr. Soc.*, **23**, 417–433.
- Fukao, Y., Widiyantoro, S. & Obayashi, M., 2001. Stagnant slabs in the upper and lower mantle transition region, *Rev. Geophys.*, in press.
- Geiger, L. & Gutenberg, B., 1912. Ueber erdbebenwellen V. *Nachr. der k. Ges. der Wiss. zu Goettingen, math.-phys. Kl.*
- Grand, S.P., 1994. Mantle shear structure beneath the America and surrounding oceans, *J. geophys. Res.*, **91**, 12 389–12 406.

- Grand, S.P., van der Hilst, R.D. & Widiyantoro, S., 1997. Global seismic tomography: A snapshot of convection in the Earth, *GSA Today*, **7**, 1–7.
- Greenfield, R.J. & Sheppard, R.M., 1969. The Moho depth variations under the LASA and their effect on $dt/d\Delta$ measurements, *Bull. seism. Soc. Am.*, **59**, 409–420.
- Hirose, K., Fei, Y.W., Ma, Y.Z. & Mao, H.K., 1999. The fate of subducted basaltic crust in the Earth's lower mantle, *Nature*, **397**, 53–56.
- Johnson, L.R., 1969. Array measurements of P velocities in the lower mantle, *Bull. seism. Soc. Am.*, **59**, 973–1008.
- Kaneshima, S. & Helffrich, G., 1998. Detection of lower mantle scatterers northeast of the Mariana subduction zone using short-period array data, *J. geophys. Res.*, **103**, 4825–4838.
- Kaneshima, S. & Helffrich, G., 1999. Dipping low-velocity layer in the mid-lower mantle: evidence for geochemical heterogeneity, *Science*, **283**, 1888–1891.
- Karki, B.B., Stixrude, L. & Crain, J., 1997. Ab initio elasticity of three high-pressure polymorphs of silica, *Geophys. Res. Lett.*, **24**, 3269–3272.
- Kawakatsu, H. & Niu, F., 1994. Seismic evidence for a 920-km discontinuity, *Nature*, **371**, 301–305.
- Kennett, B.L.N. & Engdahl, E.R., 1991. Travel times for global earthquake location and phase identification, *Geophys. J. Int.*, **105**, 429–465.
- Kesson, S.E., Fitzgerald, J.D. & Shelley, J.M.G., 1994. Mineral chemistry and density of subducted basaltic crustal lower-mantle pressures, *Nature*, **372**, 767–769.
- Kingma, M.J., Cohen, R.E., Hemley, R.J. & Mao, H.K., 1995. Transformation of stishovite to a denser phase at lower mantle pressures, *Nature*, **374**, 243–245.
- le Stunff, Y., Wicks, C.W. & Romanowicz, B., 1995. P'P' precursors under Africa: evidence for mid-mantle reflectors, *Science*, **270**, 74–77.
- Mao, H.K., Shu, J., Fei, Y., Hu, J. & Hemley, R.J., 1996. The wustite enigma, *Phys. Earth planet. Inter.*, **96**, 135–145.
- Mohorovicic, S., 1916. Die reduzierte laufzeitkurve und abhangigkeit der herdtiefe usw, *Gerlands Beitr. zur Geophysik*, Bd. XIV.
- Montagner, J.-P., 1994. Can seismology tell us anything about convection in the mantle, *Rev. Geophys.*, **32**, 115–137.
- Niu, F. & Kawakatsu, H., 1997. Depth variation of the mid-mantle seismic discontinuity, *Geophys. Res. Lett.*, **24**, 429–432.
- Oreshin, S., Vinnik, L., Treussov, A. & Kind, R., 1998. Subducted lithosphere or 530 km discontinuity?, *Geophys. Res. Lett.*, **25**, 1091–1094.
- Petersen, N., Gossler, J., Kind, R., Stammler, K. & Vinnik, L., 1993. Precursors to SS and structure of transition zone of the north-western Pacific, *Geophys. Res. Lett.*, **20**, 281–284.
- Pushcharovskii, Yu.M. & Pushcharovskii, D.Yu., 1999. Geospheres in the earth's mantle, *Geotectonics*, **33**, 1–11.
- Repetti, W.C., 1930. New values for some of the discontinuities in the earth, *PhD thesis*, St. Louis University, St. Louis.
- Tanimoto, T., 1990. Predominance of large-scale heterogeneity and the shift of velocity anomalies between the upper and the lower mantle, *J. Phys. Earth*, **38**, 493–509.
- Tromp, J. & Dziewonski, A.M., 1998. Geoscience—Two views of the deep mantle, *Science*, **281**, 655–656.
- Tsuchida, Y. & Yagi, T., 1989. A new, post-stishovite high-pressure polymorph of silica, *Nature*, **340**, 217–220.
- Vinnik, L.P. & Nikolayev, A.V., 1970. The velocity profile of the lower mantle from direct measurements of $dt/d\Delta$, *Phys. Solid Earth*, **11**, 699–708.
- Vinnik, L.P., Lukk, A.A. & Nikolayev, A.V., 1972. Inhomogeneities in the lower mantle, *Phys. Earth planet. Inter.*, **5**, 328–331.
- Vinnik, L.P. & Slavina, L.B., 1975. A new $dt/d\Delta$ profile for the lower mantle, *Phys. Solid Earth*, **11**, 742–743.
- Vinnik, L., Kosarev, G. & Petersen, N., 1996. Mantle transition zone beneath Eurasia, *Geophys. Res. Lett.*, **23**, 1485–1488.
- Vinnik, L., Niu, F. & Kawakatsu, H., 1998. Broadband converted phases from midmantle discontinuities, *Earth Planets Space*, **50**, 987–997.
- Wessel, P. & Smith, W.H.F., 1995. New version of the Generic Mapping Tools released, *EOS, Trans. Am. geophys. Un.*, **76**, 329.
- Wicks, C.W. & Richards, M.A., 1993. Seismic evidence for 1200 km discontinuity, *EOS, Trans. Am. geophys. Un.*, **43**, Suppl., 550.
- Wicks, C.W. & Weber, M., 1996. Seismic evidence for a fossil subduction zone beneath the Philippine plate, *Ann. Geophys.*, **14**, Suppl., 45.